Raymo, M.E., Jansen, E., Blum, P., and Herbert, T.D. (Eds.), 1999
Proceedings of the Ocean Drilling Program, Scientific Results, Vol. 162

17. THE DEPOSITIONAL ENVIRONMENT OF THE WESTERN SVALBARD MARGIN DURING THE LATE PLIOCENE AND THE PLEISTOCENE: SEDIMENTARY FACIES CHANGES AT SITE 986[1]

Carl Fredrik Forsberg,[2,3] A. Solheim,[2,4] Anders Elverhøi,[5] Eystein Jansen,[6] J.E.T. Channell,[7] and Espen Sletten Andersen[8]

ABSTRACT

Site 986 was drilled to 965 meters below seafloor (mbsf) on the western Svalbard margin to record the onset of glaciations and to date and document the glacial evolution in the Svalbard–Barents Sea region during the Pliocene–Pleistocene. In this paper, results of sedimentological analyses are discussed in light of seismic stratigraphy and new age determinations. The latter were difficult to obtain in the glacial deposits, and datums are sparse. Through combined paleomagnetic data, biostratigraphy, and Sr isotopes, however, an overall chronology for the main evolutionary steps is suggested. The cored sequence at Site 986 is younger than 2.6 Ma, and the lower 60 m of the section contains no evidence of a major glacial influence. An initial glaciation is interpreted to have occurred at ~2.3 Ma, resulting in increased sand deposition from debris flows at Site 986 and forming a prominent seismic reflector, R7. However, glaciers probably did not reach the shelf break until ~1.6–1.7 Ma (Reflector R6), after which the depositional environment was dominated by diamictic debris flows. A gradual change in source area from the Barents Sea to Svalbard is recorded primarily by changes in carbonate and smectite content, ~355 mbsf (Reflector R5), at an interpolated age of 1.4–1.5 Ma. During the last ~1 m.y., Site 986 has undergone more distal deposition as the main depocenters have shifted laterally. This has resulted in less frequent debris flows and more turbidites and hemipelagic deposits, with a slight fining upward of the cored sediments.

INTRODUCTION

Multichannel seismic data along the western Barents Sea and Svalbard margin (Fig. 1) have recently allowed the establishment of a seismic stratigraphy for nearly the entire margin (Faleide et al., 1996; Hjelstuen et al., 1996; Fiedler and Faleide, 1996). Seven regional seismic sequence boundaries, R7–R1, were identified, of which the deepest, R7, was interpreted to represent the base of the glacial deposits (Faleide et al., 1996). The chronology of the seismic units has been uncertain and primarily based on ties to commercial wells and shallow boreholes on the outer southwest Barents Sea shelf. A late Pliocene age of ~2.5 Ma has been suggested for R7 (Eidvin and Riis, 1989; Eidvin et al., 1993; Sættem et al., 1994).

Mass balancing the sedimentary wedge found above R7 with assumed drainage areas in the Barents Sea has led to the conclusion that glacial erosion of the Barents Sea varied from 500 m in the southern parts to >1500 m in the northern parts for the last 2.5 m.y. (Fiedler and Faleide, 1996; Hjelstuen et al., 1996). The major depocenters for the denudation products form glacial fans in front of bathymetric troughs that cross the continental shelf. Sediment thicknesses above R7 reach 4 km in the Bear Island Fan (Fig. 1) (Hjelstuen et al., 1996). A possible consequence of the high glacial denudation rates in the Barents Sea is the transition from a primarily subaerial platform to a primarily submarine platform. This has been suggested by Rasmussen and Fjeldskaar (1996) and also by Bråten (1997), on the basis of isostatic modeling.

Site 986 was drilled to penetrate the glacial sequences and thereby record and date the paleoclimatic and depositional changes that occurred during the Pliocene–Pleistocene in this region. This is the first site drilled directly into the continental slope/rise environment on this continental margin. The main objectives of the present study are to identify the main sedimentary facies changes present on the western Svalbard margin and to interpret them with respect to the glacial history of the region.

MATERIALS AND METHODS

Shipboard measurements and sediment descriptions (Table 1; Shipboard Scientific Party, 1996) provide the background information and basic stratigraphy used in the present study. To fulfill the objectives of the study, a sample coverage as even as possible throughout the hole was selected, with an optimum of one 10-cm^3 sample per section (i.e., one sample every 1.5 m in the recovered cores) (Fig. 2). All samples were subjected to grain-size analyses, mineralogical analyses, and total organic carbon and carbonate analyses.

Grain-Size Analyses

Two sets of grain-size analyses were performed (Fig. 2). One set of 305 samples (10 cm^3) consisted of sieving the material coarser than 63-µm fraction and settling analyses, using a Sedigraph 5000D, of the silt and clay fractions. The other set was obtained by sieving 592 shipboard physical properties samples (3–5 cm^3) but gave only the total fraction finer than 63-µm, the 63- to 500-µm, and the >500-µm fractions.

Total Carbon and Carbonate Analyses

The carbon and carbonate contents were found by analyzing both untreated and acid-leached samples of dried and ground sediments in a LECO 5344 furnace. The carbon content in the acid-leached samples represents the total organic carbon (TOC), whereas the difference between the total carbon (TC) in the untreated samples and the

[1]Raymo, M.E., Jansen, E., Blum, P., and Herbert, T.D. (Eds.), 1999. *Proc. ODP, Sci. Results*, 162: College Station, TX (Ocean Drilling Program).
[2]Norwegian Polar Institute, P.O. Box 5072, Majorstua, N-0301 Oslo, Norway.
[3]Saga Petroleum, P.O. Box 490, N-1301 Sandvika, Norway. carl.forsberg@saga.com
[4]Aker Geo Seismic AS, FjordallTen 16, P.O. Box 1884, Vika, N-0124 Oslo, Norway.
[5]Department of Geology, University of Oslo, P.O. Box 1047, Blindern, N-0316 Oslo, Norway.
[6]Department of Geology, University of Bergen, Allégaten 41, N-5007 Bergen, Norway.
[7]Department of Geology, University of Florida, Gainesville, FL 32611, U.S.A.
[8]Norsk Hydro ASA, P.O.Box 200, N-1321 Stabekk, Norway.

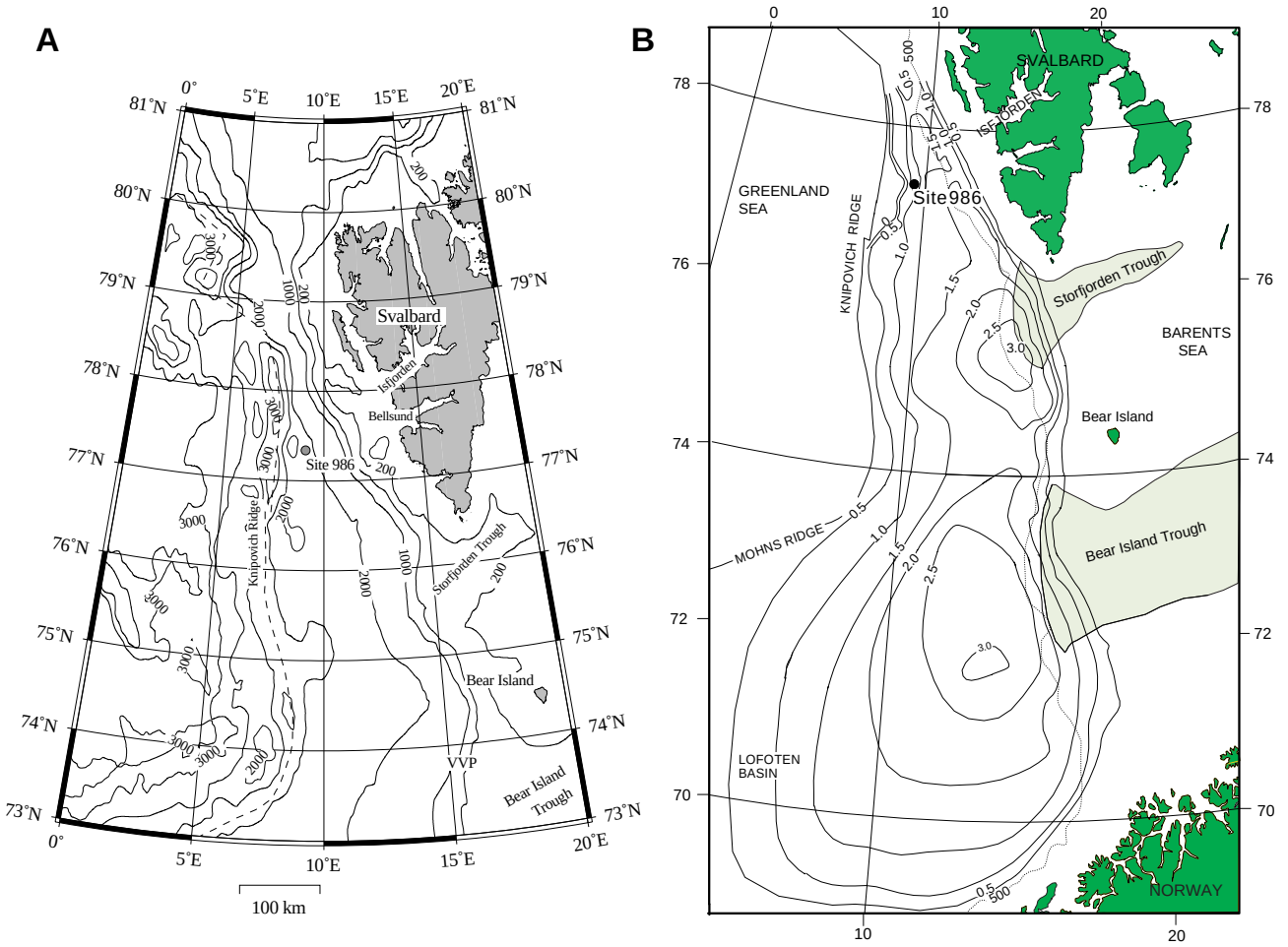

Figure 1. **A.** Bathymetric map showing location of Site 986. VVP = Vestbakken Volcanic Province. The dashed line marks the Knipovich Ridge spreading axis. **B.** Total thickness (in seconds of two-way traveltime) of upper Cenozoic sediments, R7 to the surface, showing major depocenters outside Storfjorden and Bear Island Troughs (adapted from Faleide et al., 1996). Site 986 is located between the smaller glacial fans off Isfjorden and Bellsund (A).

Table 1. The appearance of Site 986 lithologic units based on core descriptions.

Unit	Subunit	Depth (mbsf)	Thickness (m)	Lithology and characteristic features
I		0-98	98	Silty clay and clay with silt interbedded with nannofossil mixed sediment and silty clay with nannofossils. Moderate amounts of clasts. Common sandy layers.
II		98-561.8	463.8	Silty clay with minor occurrence of clay with silt. Few silty clay intervals with inorganic calcite and/or sand. Dominant clast content. Mostly without biogenics. Highly variable natural gamma radiation and magnetic susceptibility throughout the unit. Common sandy layers.
III		561.8-820.3	258.5	Clayey silt with sand, silty clay with sand, and clayey silt with nannofossils. Sediment is hard and fractured throughout the interval. High sand content although clasts nearly absent. Common contorted intervals and variably inclined beds (0°–70°).
IV	IVA	820.3-897.3	77	Silty clay with sand, minor occurrence of clay with silt. Nearly barren in clasts, few nannofossils. Common slump structures and variably inclined beds (10°-70°).
IV	IVB	897.3-964.6	67.3	Silty clay, nearly barren in clasts and no biogenics. Very low sand content.

Note: Data are from Shipboard Scientific Party (1996).

TOC was attributed to carbonate lost during the leaching process. A total of 305 TOC/TC analyses were performed (Fig. 2).

X-Ray Diffraction Analyses

Both unoriented ground bulk samples and oriented samples of the clay-sized fraction were analyzed. Diffractograms were produced using a Philips PW17129 X-ray diffractometer and recorded both digitally and on paper. X-ray diffraction (XRD) analyses are only semi-quantitative, the results being subjected to both experimental errors introduced during sample preparation and errors produced by the conversion of X-ray counts to mineral percentages. The latter results from variability in the signature of individual minerals. These are not known at this site, and we have not converted X-ray counts to mineral percentages using weighting factors. The quantification is based on the total number of counts under selected peaks, between the peak half-heights after the background level has been subtracted. Only relative changes in mineralogical composition will therefore be appar-

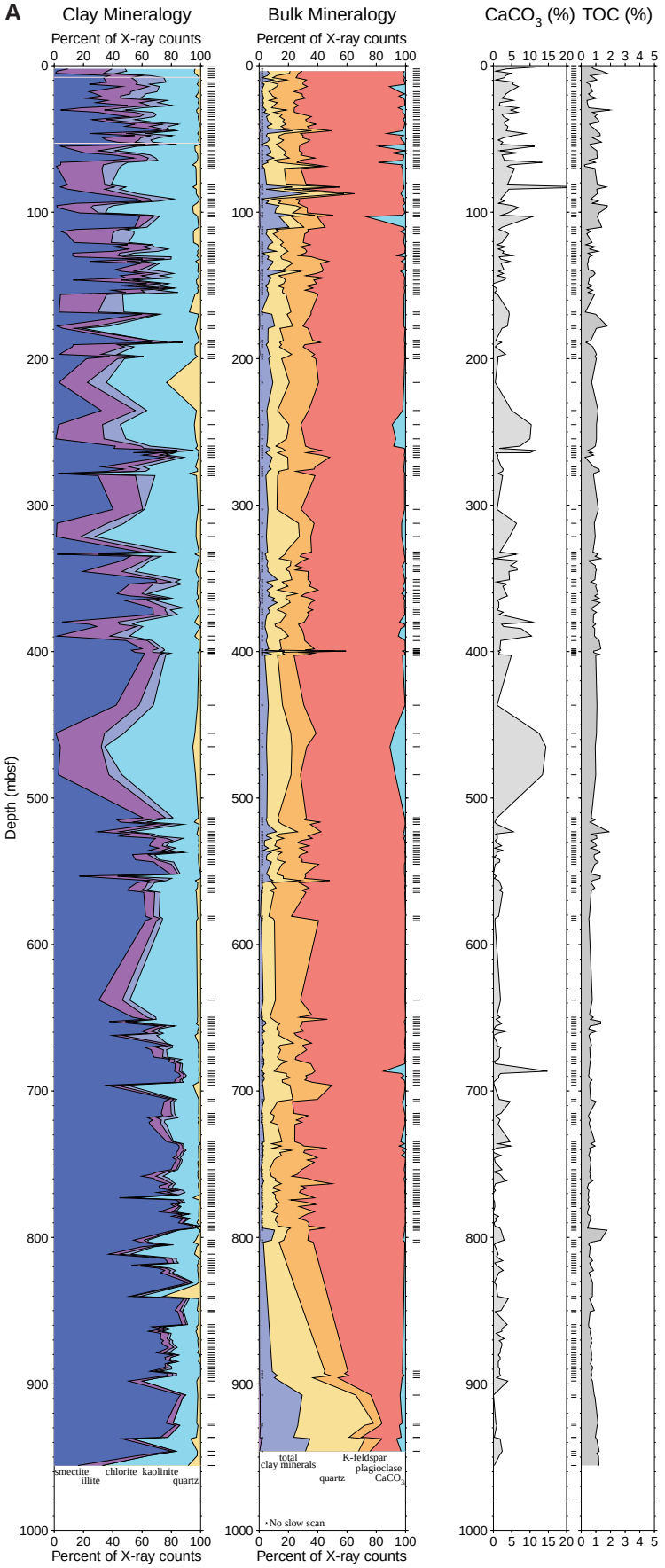

Figure 2. Summary of results plotted vs. depth (mbsf) for (**A**) clay and bulk mineralogies and (**B**) grain size. Both the clay and bulk mineralogies reflect the number of X-ray counts under the peaks used for quantification. No weighting factors have been used. The grain-size profile is a combination of analyses performed on both the offshore physical properties samples (3–5 cm^3) and separate samples (10 cm^3) requested for postcruise analyses. Densities are from both discrete offshore density measurements (points) and the wireline density log (shaded curve) (Shipboard Scientific Party, 1996). The reflectors and units are those defined by Faleide et al. (1996) and Shipboard Scientific Party (1996). The horizontal bars next to the mineralogical and grain-size results and between the TOC and TC columns show where samples have been analyzed. Recovery is indicated by black shading. (Continued on next page.)

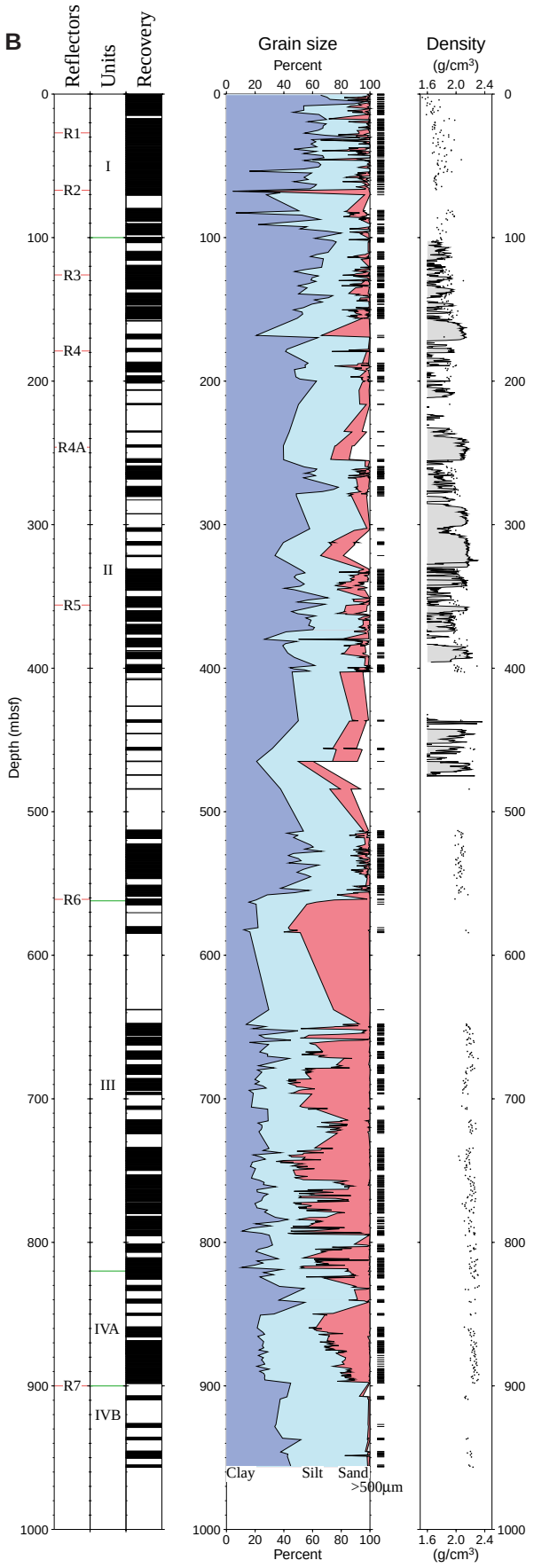

Figure 2 (continued).

ent. Whereas the main mineralogical composition was found by manual interpretation and comparisons, the quantification was automated on a computer using a UNIX script written for this purpose as part of the study. Peaks from the various scans (Fig. 3) were used in the quantification process (Table 2) and normalized to a sum of 100%. The reproducibility of multiple diffractograms from the same XRD slide is good with an estimated maximum difference of <5%. XRD analyses on different slides from the same sample give results agreeing within ~10%–15%.

The 261 bulk samples were ground for 1.5 to 2 min in an automatic steel mill and mounted in aluminum powder holders using a side packing technique. A normal scan between 2° and 45° 2θ (0.06° per step, 3 s sample time) and a slow scan between 26° and 29° 2θ (0.01° per step, 4 s sample time) were recorded. θ is the angle of incidence of the X-rays on the sample.

The clay-sized samples were filtered on Millipore filters and inverted onto silica plates. Scans were performed of samples that were untreated, glycolated, and heat treated at 300°C and also at 550°C (Fig. 3). Slow scans between 24° and 26° 2θ were also obtained to separate the chlorite 004 and kaolinite 002 peaks.

$^{87}Sr/^{86}Sr$ Ratios

Sr isotope ratios were determined using a Finnigan MAT 262 mass spectrometer at the University of Bergen. The samples analyzed were composed of either a mixture of planktonic (*Neogloboquadrina* spp. and *Globigerina bulloides*) or mixed benthic foraminifers. Because of the low number of specimens, there was not enough material for single-species analyses. The values are adjusted to a value for NBS 987 Sr standard of 0.710240. Estimated sample reproducibility is $\pm 2 \times 10^{-6}$. To calculate ages on the basis of the Sr vs. age relationship of Howarth and McArthur (1997), we adjusted the values by +0.000008 before calculating ages, to reflect the difference between the NBS 987 values used in this work (0.710248) and our value for this standard (0.710240). To calculate ages on the basis of the Hodell et al. (1991) and Farrell et al. (1995) Sr time scales, one needs to adjust the values by –0.000005 before calculating ages, to reflect the difference between the NBS 987 values used in these papers (0.710235) and our value for this standard (0.710240).

RESULTS

The results are presented stratigraphically from the base of the drilled section and upward within the lithostratigraphic framework provided by the Shipboard Scientific Party (1996) (Table 1). This allows the presentation of similarities and differences between the different units. The interpreted cause of these differences will be presented in the discussion.

Subunit IVB, a silty clay with thin bedding, is distinguished from Subunit IVA, which is a silty clay with sand with contorted and/or variably inclined bedding (10°–70°) (Shipboard Scientific Party 1996). The transition from Subunit IVB to Subunit IVA at 900 meters below seafloor (mbsf) (Reflector R7; Figs. 2, 4) is seen as an increase in the sand content from 2%–3% to 20%–40%. However, both units have only a minor (<0.5%) content of material coarser than 500 µm (Fig. 2). The changes in bulk mineralogy (decrease in total clay minerals; Fig. 2) and the decrease in total organic carbon can be attributed to the change in grain size. The clay mineralogy (Figs. 2, 5) is dominated by smectite and chlorite/kaolinite and remains basically unchanged at the boundary. The carbonate content increases marginally into Subunit IVA. The sand content increases through Subunit IVA to the base of Unit III.

Unit III consists of poorly sorted sediments containing varying amounts of clay, silt, and sand but with an average of ~40% sand and 30% of both clay and silt (Fig. 2). These sediments are interlayered with deposits containing less sand as exemplified by the intervals ~800 mbsf and 760 mbsf. Undisturbed sediments are described

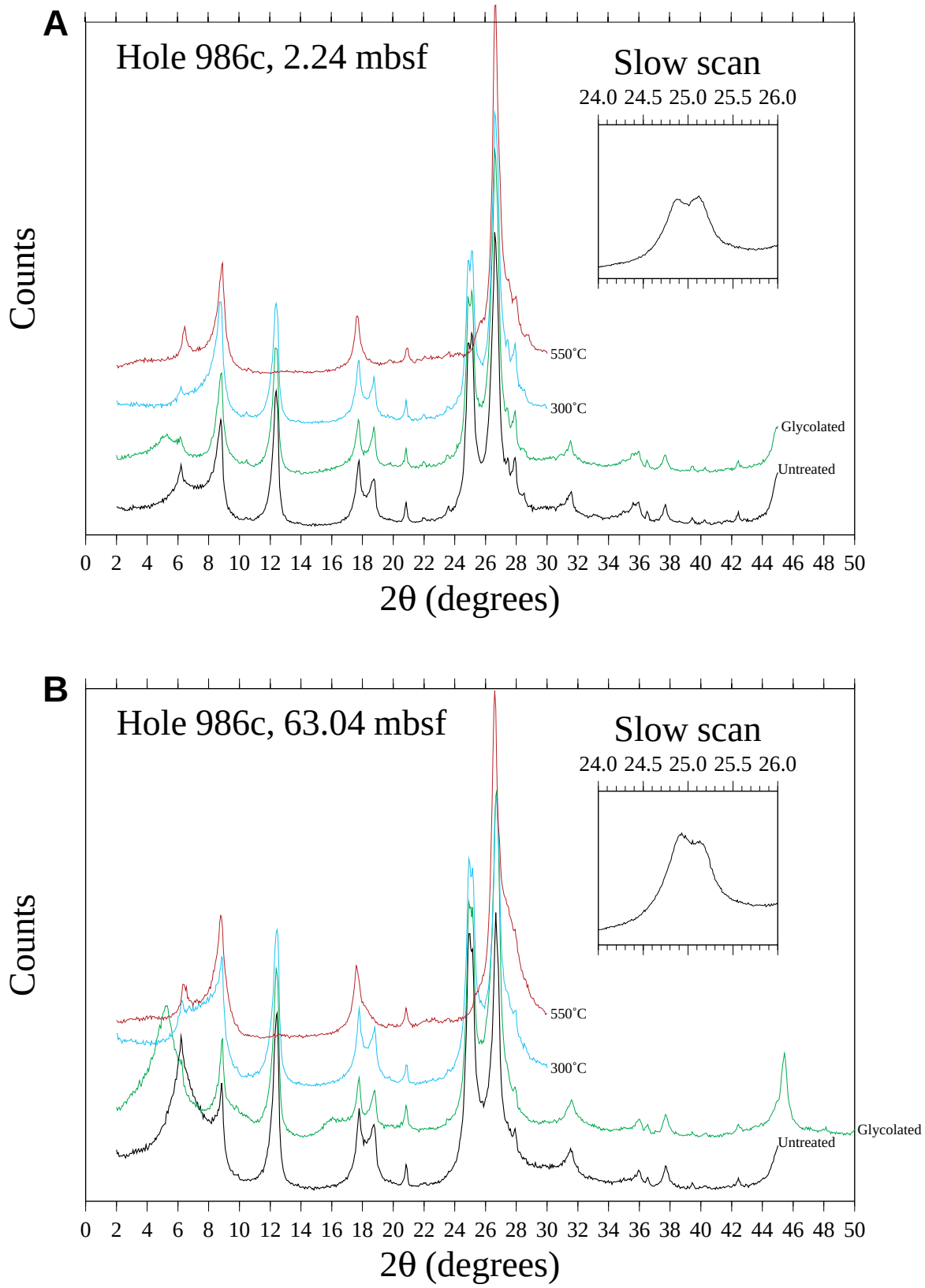

Figure 3. Typical X-ray diffractogram series for determination of clay mineralogy for **(A)** a sample with little smectite (~9%) and **(B)** a sample with a significant smectite content (~54%). Each figure shows the untreated curve along with both the glycolated curve, heat treated at 300°C, and the curve heat treated at 550°C, successively shifted upward (in this order) by 1500 counts. The length of the counts axis is 15,000 counts. Table 2 shows which peaks are used for identification and quantification.

Table 2. Peaks used to identify and quantify minerals from X-ray diffractograms of bulk and clay-sized fractions.

Mineral	Identification	Peak for quantification	Comments
Smectite	Expansion after glycolation of 14 Å peak to ~17 Å. Collapse to 10 -14 Å after heating to 330°C.	17 Å (5.2°2θ) glycolated	Clay mineralogy
Chlorite	14 Å peak on glycolated run and peak on untreated slow scan	14 Å (6.2°2θ) heated to 550°C	Clay mineralogy
Illite	10 Å glycolated	10 Å (8.8°2θ) glycolated	Clay mineralogy
Kaolinite	7 Å peak and peak on slow scan	7 Å (12.4°2θ) glycolated minus 14Å (6.2°) heated to 550°C	Clay mineralogy
Quartz	4.26 Å	4.26 Å (20.8°2θ) untreated	Clay and bulk mineralogy
Total clays	4.48 Å (19.8°2θ)	4.48 Å (19.8°2θ)	Bulk mineralogy
K-feldspar	3.25 Å (27.42°2θ)	3.25 Å (27.42°2θ)	Bulk mineralogy
Plagioclase	3.18 Å (28.04°2θ)	3.18 Å (28.04°2θ)	Bulk mineralogy
Calcite	3.03 Å (29.5°2θ)	3.03 Å (29.5°2θ)	Bulk mineralogy

(Shipboard Scientific Party, 1996) as containing contorted regions and bedding at various inclinations (0°–70°). The mineralogy of Unit III is the same as that of Subunit IVA.

The transition from Unit III to Unit II is associated with the first persistent appearance of clasts in the core (Shipboard Scientific Party, 1996), an increase in the clay content to ~30%, and a reduction in the sand content to between 5% and 20% (Figs. 2, 4). For the units overlying Unit III, there is a general fining upward trend, interrupted by coarse layers with a high (>500 µm) clast content, reaching as much as 40%. Sample recovery was poor in these coarse layers, which are seen as high-density (as much as 2.2 g/cm^3) intervals on the wireline density plot (Fig. 2). They were interpreted as debris flow deposits by the Shipboard Scientific Party (1996).

The greatest change in the bulk mineralogy across this boundary is apparent in the total clay content, but a large increase in the carbonate content, seen in both in the XRD results and the carbonate curves (Figs. 2, 6), is apparent in conjunction with the high content of the >500 µm–sized fraction beginning at 485 mbsf. Above this level in Unit II, abundant peaks in the carbonate content of as much as 10%–20% are apparent. The clay mineralogy is more variable in Unit II than in Unit III, the most obvious variation being in the smectite content. Between 560 (R6) and 355 mbsf (R5), two main characteristic sediment types appear to be present: coarse, high-density, carbonate-rich, smectite-poor deposits with finer, smectite-rich layers in between (Fig. 2). However, even in the smectite-rich intervals, there is less smectite and more illite than in the units below.

The ternary diagrams (Fig. 5) show that the coarse sediments with lower smectite content first appear above 560 mbsf (R6). A more subtle change is also evident at about the level of 355 mbsf (R5). Above 355 mbsf, the clay mineralogy seems to have no relation to the coarse fraction (>500 µm) content, whereas this seems to be the case below. Several random mixtures of two sediment types will produce a linear trend on a plot of the resultant mineralogical composition in a ternary diagram. The linear trend apparent on the diagrams for the sediments above 355 mbsf can therefore be taken as an indication of a mixing of two sediment types. The two end types may be considered to be smectite rich (75% smectite, 20% chlorite/kaolinite, and 5% illite counts) and smectite poor (5% smectite, 60% chlorite/kaolinite, and 35% illite counts).

$^{87}Sr/^{86}Sr$ Age Determinations

The results are tabulated in Table 3. The $^{87}Sr/^{86}Sr$ values vary between 0.709131 and 0.709067. There is a pronounced scatter that may stem either from analytical problems, such as contamination, or from various effects of redeposition of older specimens.

We employed the Sr isotope vs. age statistics of Howarth and McArthur (1997) to derive ages from the Sr isotope values (Table 3). This technique uses the Cande and Kent (1995) time scale and a LOWESS fit to the Sr data, and it also provides age limits for the 95% confidence interval (see Table 3). We prefer the Howarth and McArthur (1997) age model because it is based on newer and more comprehensive statistics. This method gives, in general, ages in between those obtained by using the Sr vs. age relationship of Hodell et al. (1991) and that of Farrell et al. (1995), but the results are closer to the Hodell et al. (1991) fit. The Farrell et al. (1995) fit provides significantly older ages but also very wide error bars for those samples with the lowest Sr ratio. This is caused by the polynomial fit of the Sr vs. age relationship used by Farrell et al. (1995). The polynomial fit is very flat in the age interval 2.7–4 Ma; hence, ages older than 2.6–2.7 Ma are very uncertain.

CORRELATION WITH SEISMIC SECTIONS

Based on combined shore-based lithologic analyses and shipboard physical properties measurements (Shipboard Scientific Party, 1996), the seismic reflections are caused primarily by variations in grain-size distribution, which again cause changes in both the wet bulk density and the *P*-wave velocity. Such variations give rise to the seismic sequence boundaries, as well as the internal seismic reflections within the sequences. R7 is caused by the main upsection increase in the sand content (Fig. 2), which gives rise to increases in both density and velocity and therefore sets up a negative acoustic impedance contrast. A relatively homogeneous density structure within the R7–R6 sequence gives rise to few and weak internal reflections around Site 986. A more stratified character eastward may result from a higher hemipelagic influence on the continental slope.

R6 marks the change from a relatively homogeneous sandy, silty sequence to the much more variable lithologies above. In particular, differences in clast and sand content, which most often are related to distinct debris flow units (Shipboard Scientific Party, 1996), cause large density differences (Fig. 2). These set up frequent acoustic impedance contrasts that give rise to the acoustically stratified structure above R6 (Fig. 7). Solheim et al. (1998) present single-channel seismic lines running both parallel and perpendicular to the continental slope that clearly show the discontinuous and commonly lobe-shaped nature of these reflecting horizons. Apparently weaker and less abundant reflections toward the top of the section result from a response to a decrease in the number of debris flows and to a generally fining-upward trend in the lithology at this site, with less significant density and velocity variations (Fig. 2) (Shipboard Scientific Party, 1996).

DISCUSSION

The unraveling of the depositional history of this area is limited in detail by the resolution available in the chronological studies. The recovery at the site has many gaps (Fig. 2), but an adequate coverage of all the lithostratigraphic units has been obtained. We therefore begin this discussion by presenting our interpretations of the facies changes seen at the site and continue with a discussion of the chronology in light of these interpretations. Finally, we indicate mineralogical problems that remain unresolved and that need to be addressed in more detail.

Facies Changes

Subunit IVB has a grain-size distribution and a thinly bedded structure compatible with a hemipelagic sediment. The absence of

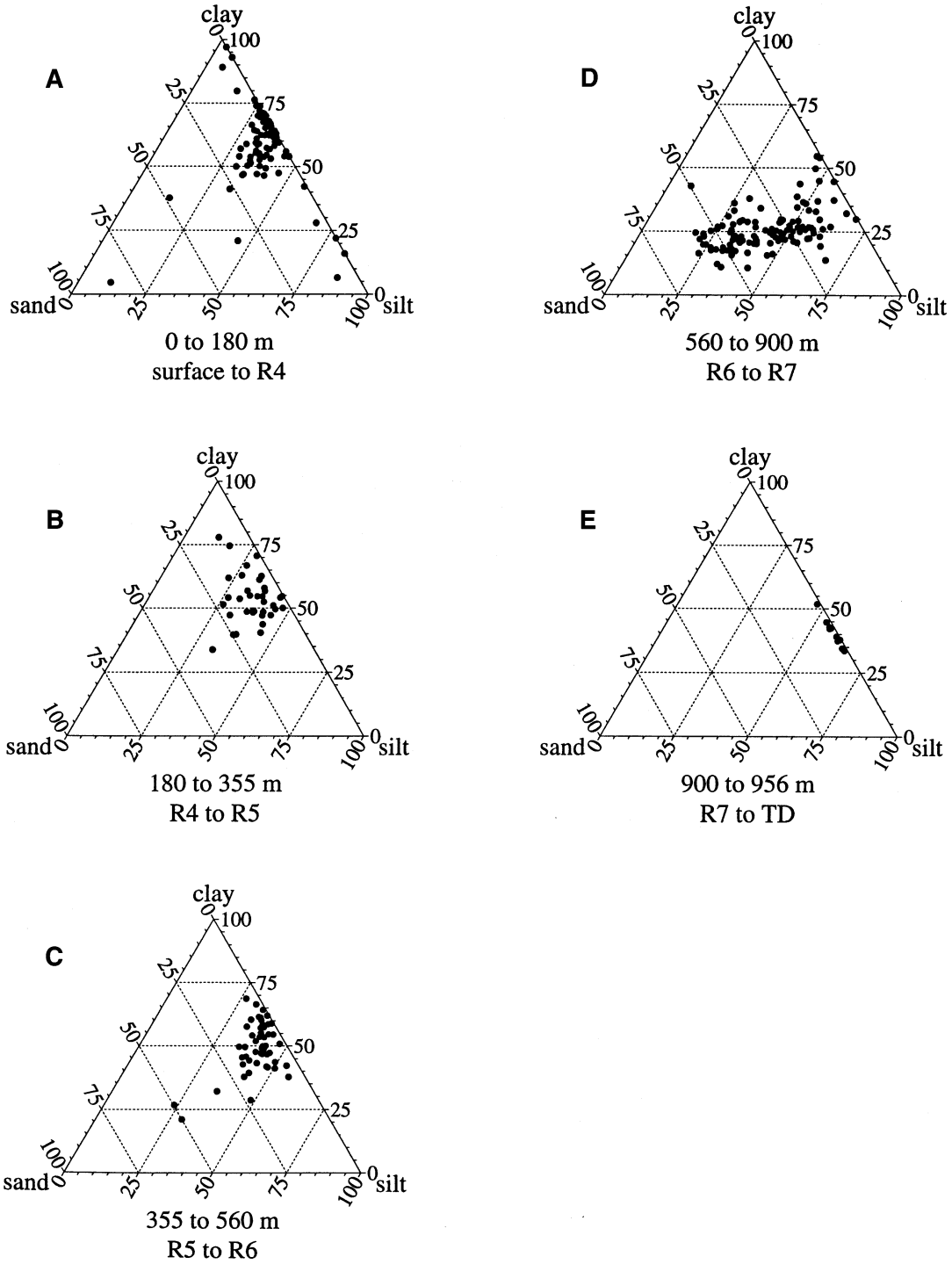

Figure 4. Diagrams of grain-size distribution between seismic reflectors. The fine sediments below R7 **(E)**, the sandy interval between R6 and R7 **(D)**, and the fining upward above R4 **(A, B, C)**, seen as a clustering of results along the clay-silt axis in (A), are demonstrated.

clasts and the paucity of material coarser than 500 µm lead us to interpret this unit as a sediment deposited under limited (or insignificant) glacial influence.

The transition between Subunit IVB and Subunit IVA is correlated to Reflector R7 (Shipboard Scientific Party 1996), which has previously been identified as the base of the glacial sequences (2.3 Ma) (Hjelstuen et al., 1996; Faleide et al., 1996). At Site 986, this transition is associated with a an increase in the sand content. It rises up through Subunit IVA to Unit III, where it remains generally high (~40%) but is interlayered with a few zones with <20% sand (Fig. 2). The sediments in Subunit IVA and Unit III, however, do not usually contain clasts. This is problematic, as glaciations are traditionally associated with the deposition of ice-rafted debris in the form of clasts. Subunit IVA and Unit III are, however, described as massive, with soft sediment deformation structures, and containing contorted and/or variably inclined bedding (Shipboard Scientific Party 1996). No graded beds are described. We interpret these structures combined with the sediments' poor sorting as indicative of downslope mass

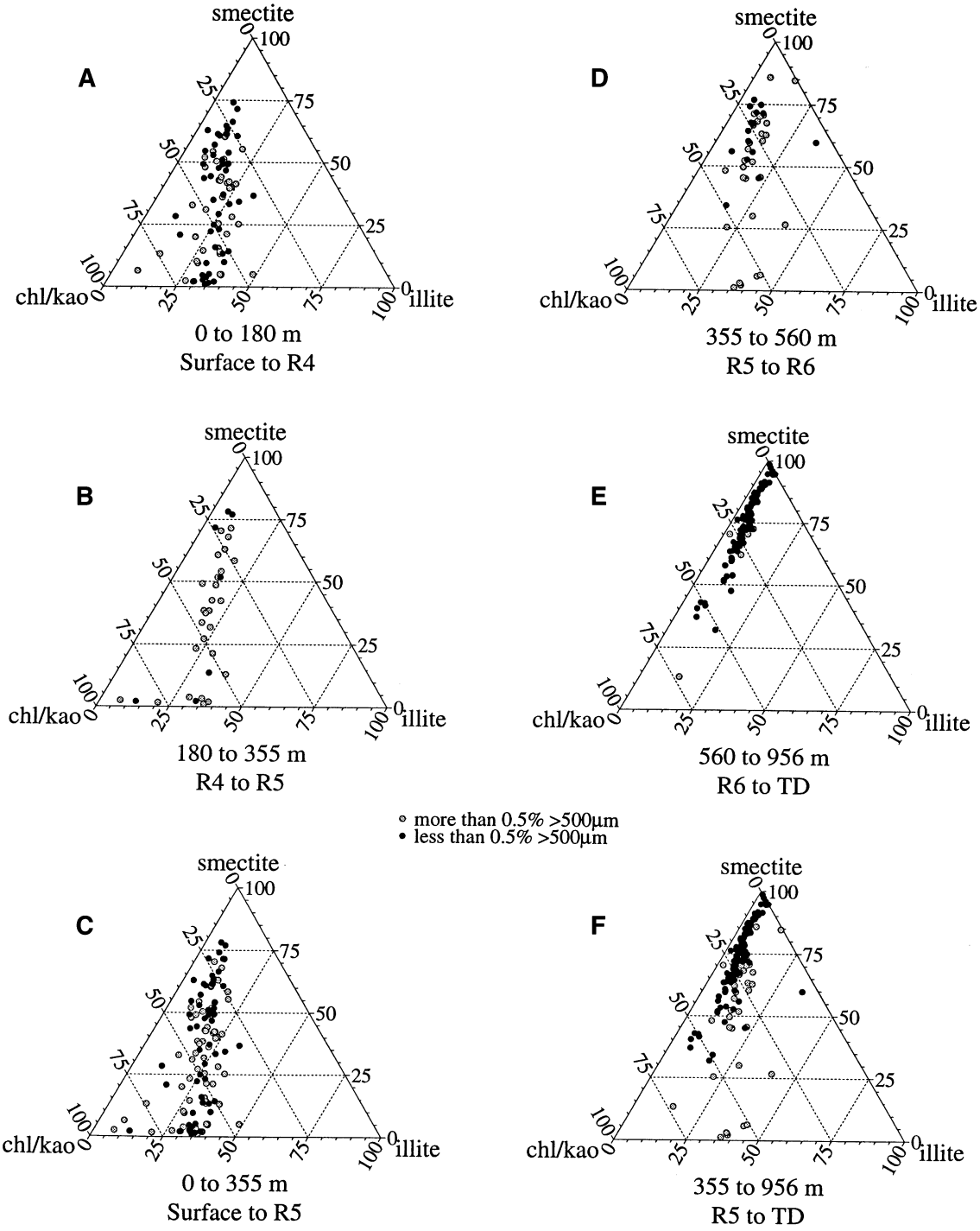

Figure 5. The mineralogy of the clay-sized fractions from X-ray diffractograms. Chl/kao is the sum of the chlorite and kaolinite contents. (**C**) is the total of (**A**) and (**B**), whereas (**F**) is the total of (**D**) and (**E**). Black circles represent samples containing <0.5% by weight of the size fraction >500 µm (i.e., the more fine grained sediment). Gray circles are those with >0.5% (i.e., the more coarse grained deposits). The dominance of smectite in the fine sediments below R6 is shown in (E). The difference in smectite content in the clay fraction between the fine- and coarse-grained samples is seen in (D). This difference cannot be seen in (A) or (B).

transport (e.g., debris flow deposits or possibly turbidites). However, the lack of grading and traction features would seem to preclude the latter. The high smectite content (Fig. 2) gives the sediment thixotropic properties conducive to movement as debris flows. The sand-poor intervals within these units are interpreted to be from periods with hemipelagic sedimentation between the debris flows. Eiken and Hinz (1993) propose on the basis of seismic interpretations that the interval between the R7 and R6 reflectors, which at this site is considered to consist of Subunit IVA and Unit III (Shipboard Scientific Party 1996), is a contourite (Bouma and Hollister, 1973; Howe et al., 1994). This interpretation is also problematic because cores are not described (Shipboard Scientific Party, 1996) as containing traction

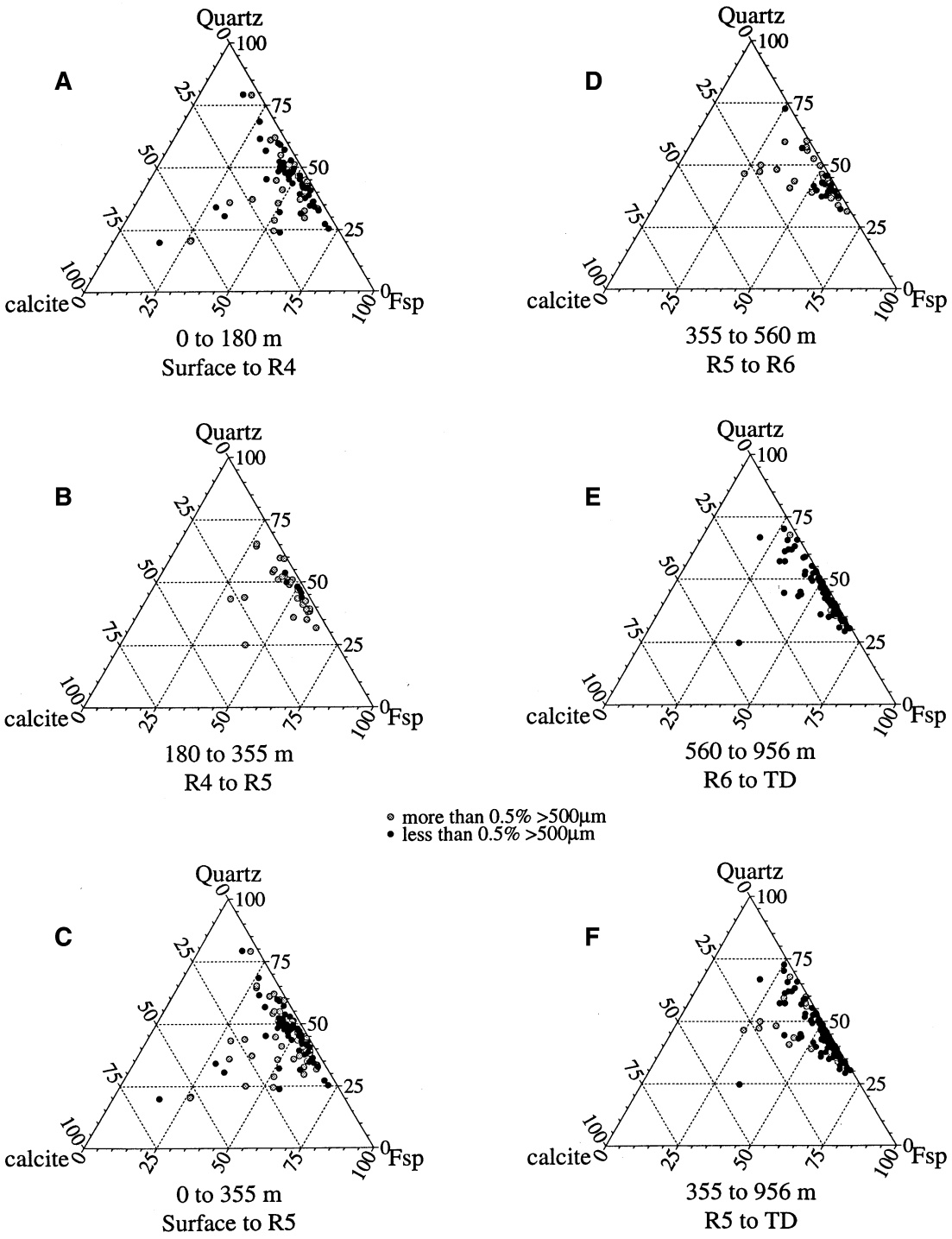

Figure 6. Bulk mineralogy from X-ray diffractograms. Fsp is the sum of K-feldspars and plagioclase. (**A**) shows a mineralogy independent of the 500-µm content. (**B**) and (**D**) demonstrate coarse layers associated with higher calcite contents. (**E**) shows the low calcite content and the predominantly fine nature of the sediments below R6. (**C**) is the total of (A) and (B), whereas (**F**) is the total of (D) and (E). Symbols are as in Figure 5.

features such as ripples, which are characteristic of bed-load transport.

We thus interpret the facies change from Subunit IVB to Subunit IVA and Unit III as a change from hemipelagic sedimentation to sedimentation dominated by debris flows or turbidites. Combined with the high sedimentation rates (see next section) in Subunit IVA and Unit III, this indicates major changes in the sedimentary processes on Svalbard and the Barents Sea. We interpret the change as a response to an initial glacial buildup on land and an accompanying increase in the rate of erosion and therefore the sediment supply to the continental margin. The paucity of clasts indicates that glaciers did not reach sea level (as opposed to the situation in Fennoscandia; Jansen and Sjoholm, 1991) at this stage and that fluvial transport of sediment to the coast was involved. One may therefore speculate that such a flu-

vial system built a delta-fan complex onto the continental margin and slope.

Assuming that Unit III and Subunit IVA continue to represent the interval between R7 and R6, they can be seen to thin up the continental slope on the Spitsbergen continental margin. Their seismic character changes from chaotic to laminated (Hjelstuen et al., 1996; A. Solheim et al., unpubl. data). Both these changes can be attributed to fan morphology (e.g., Reading and Richards, 1994). With a sediment supply near the depocenter of the Storfjorden fan (Fig. 1) (Hjelstuen et al., 1996) and a lateral spreading in the deep sea, an upslope thinning in distal areas is to be expected. The upslope thinning of the unit is much less pronounced near the Storfjorden Fan depocenter (Hjelstuen et al., 1996; A. Solheim et al., unpubl. data). The distribution and structure of the R6 to R7 interval is, however, being subjected to further scrutiny in an ongoing study (A. Solheim et al., unpubl. data).

Table 3. $^{87}Sr/^{86}Sr$ analyses of planktonic and benthic foraminifers from Site 986.

Core, section, interval (cm)	Foraminifer	Depth (mbsf)	$^{87}Sr/^{86}Sr$	Age (Ma)	Age limits (Ma)
162-986D-					
30R-2, 29-36	Planktonic	668.420	0.709086	1.81	1.75-1.94
35R-1, 29-31	Planktonic	714.920	0.709068	2.60	2.42-2.81
35R-1, 29-36	Benthic	714.920	0.709067	2.66	2.47-2.91
39R-6, 29-36	Planktonic	760.820	0.709089	1.73	1.61-1.84
39R-6, 29-36	Benthic	760.820	0.709071	2.43	2.26-2.62
44R-3, 29-36	Benthic	804.420	0.709077	2.14	2.00-2.29
44R-3, 29-36	Planktonic	804.420	0.709108	1.35	1.31-1.40
45R-7, 29-36	Planktonic	820.020	0.709089	1.73	1.61-1.84
45R-7, 29-36	Benthic	820.020	0.709068	2.60	2.42-2.81
53R-4, 29-36	Planktonic	892.420	0.709131	1.05	1.02-1.09

Note: Ages are determined from data of Howarth and McArthur (1997).

The clay mineralogy is similar in Subunits IVB, IVA, and Unit III. Although the source for the smectite content in recent sediments of the Barents Sea is thought to be Siberia and the Siberian continental shelf (Forsberg, 1983; Pfirman et al., 1997), a source area much closer to Site 986 is implied by the very high smectite content of the clays in Units III and IV. Weathering of volcanic ash/glass deposits often produces smectite-rich beds. Thus, both the Knipovich Ridge spreading axis to the west of the site and the Vestbakken Volcanic Province (Fig. 1) (Mørk and Duncan, 1993) to the south of Bear Island may be source areas. However, the high smectite content combined with the idea of the debris flow origin of the units suggests the continental shelf or slope near the latter as the more likely candidate. Volcanic activity in this area is interpreted to have continued into the late Pliocene (2.3 Ma) (Mørk and Duncan, 1993) and is thus compatible with the probable age at the base of Hole 986D. A change in the smectite source from the base to the top of the cored interval at the site is thus implied. This study has not, however, determined a change in smectite type within the hole, something that may be possible with more refined analyses.

The top of Unit III is associated with Reflector R6 (Shipboard Scientific Party, 1996) and marks the initial persistent appearance of clasts in the sediments. Debris flows on the slope have been associated with the advance of glaciers onto the shelf during the Weichselian glaciation and the rapid deposition of unstable sediments at the shelf break (Elverhøi et. al., 1995a, 1995b; Hooke and Elverhøi, 1996; Laberg and Vorren, 1995; Vorren and Laberg, 1997; Sejrup et al., 1996; Hiscott and Aksu, 1994; Aksu and Hiscott, 1992; King et al., 1996). The diamictons within Unit II are therefore similarly interpreted as debris flows whose appearance is taken as evidence of the first advance of the glaciers onto the shelf edge. These debris flows are seen as high-density intervals on the wireline density log (Fig. 2). Al-

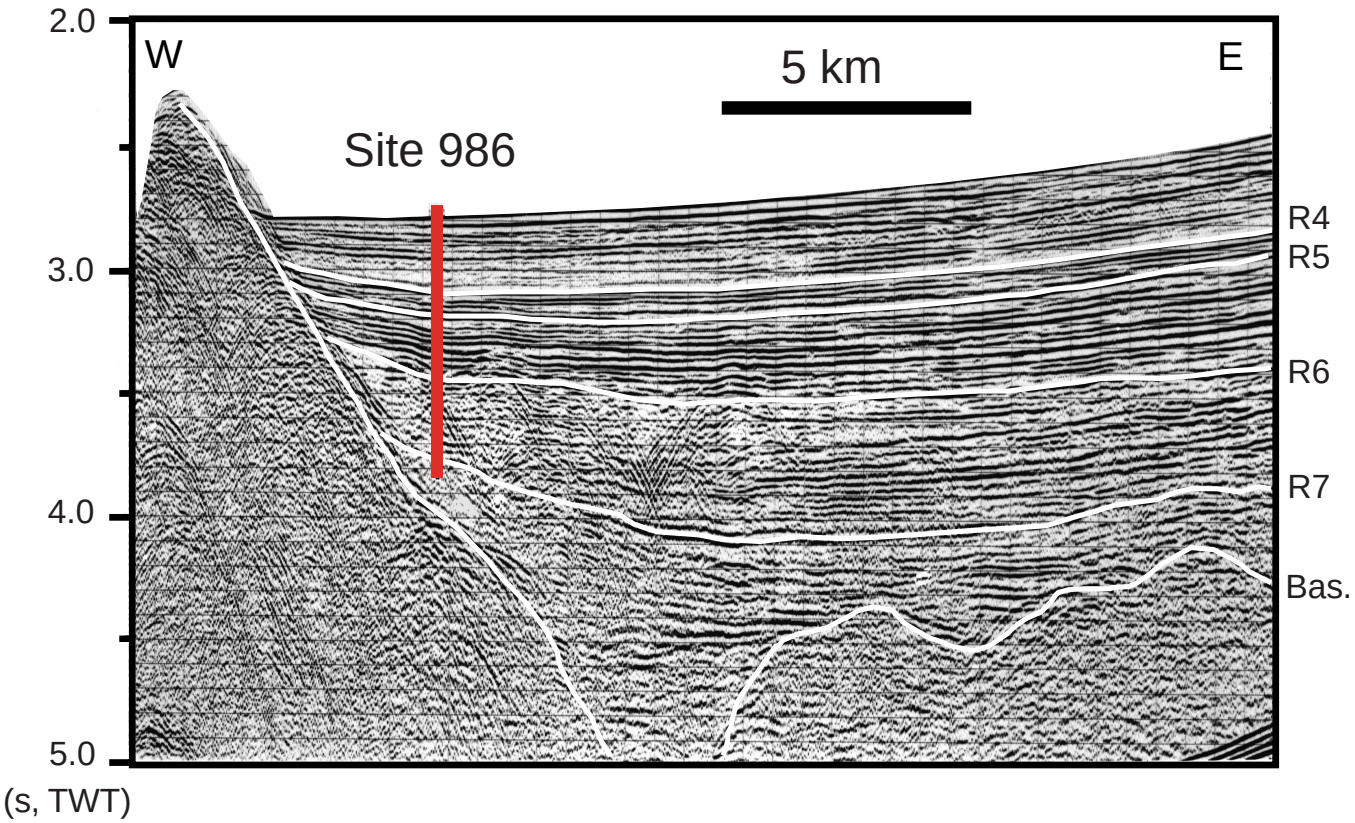

Figure 7. Sample of multichannel seismic line BEL-4, which is a dip line ~4 km to the north of Site 986. The site is projected onto this seismic line using a tie line shot during Leg 162 (Shipboard Scientific Party, 1996). Main seismic sequence boundaries R7, R6, R5, and R4, as well as the oceanic basement (Bas.), are indicated. TWT = two-way traveltime.

though these intervals are sparsely sampled, they do show that the mineralogy is different from the surrounding sediments. They have a high carbonate content and a reduced smectite content. The change in the carbonate content at 560 mbsf (R6) and the transition in the clay mineralogical composition at ~355 mbsf (R5) (Fig. 5) seem to mark a change in the source areas for the sediments deposited at Site 986. No smectite source is known from this area, although extensive carbonate outcrops exist (Flood et al., 1971). We therefore interpret this change as reflecting the increasing importance of Svalbard as a source area in conjunction with the buildup of glaciers over the archipelago.

Thus, although R5 does not manifest itself very clearly at Site 986, it does mark a significant change in the sedimentary environment on the hinterland. On seismic records from the continental slope, it forms a significant erosional unconformity that even truncates Reflector R6 in the Bear Island Fan (Faleide et al., 1996).

There is a generally fining-upward trend through Units II and I (Fig. 2), and the high-density debris flow layers decrease in thickness and intensity. Seismic records and isopach maps show that this may reflect the lateral migration of the Bellsund/Isfjorden Fan depocenter toward the south/north (Andersen et al., 1994; Solheim et al., 1996). The depositional facies at Site 986 thus becomes more distal with a transition from debris flows to turbiditic deposition. After R4 time, the Bellsund and Isfjorden fan systems are clearly discernible on the seismic records as discrete entities (Andersen et al., 1994).

Chronology

Improving the sparse age control for the Pliocene–Pleistocene of the entire Svalbard and Barents Sea margin was one of the prime reasons for drilling at Site 986. Although still somewhat limited, new age information at Site 986 results from paleomagnetic data, biostratigraphy, Sr isotope analysis, and seismic correlation (Fig. 7). The paleomagnetic information results from shipboard studies, discrete sample analyses, and postcruise analyses of the geological high-resolution magnetometer tool wireline logs (Channell et al., Chap. 10, this volume). The biostratigraphic data, on the other hand, are from the lower part of the drilled section (below 647 mbsf) and are based on Eidvin and Nagy (Chap. 1, this volume).

The Brunhes/Matuyama boundary is found at 133 mbsf (Channell et al., Chap. 10, this volume), which coincides with regional seismic Reflector R3 (Faleide et al., 1996). The top of the Jaramillo Subchron centered at 152 mbsf is observed both in the core data and in the wireline logs (Channell et al., Chap. 10, this volume). Although still uncertain, this indicates an age of between 1.0 and 1.2 Ma for Reflector R4, after which a shift in depocenter location is reported by Solheim et al. (1996). The paleomagnetic analyses indicate a normal polarity zone interpreted to be the Olduvai Event at between 735 and 755 mbsf (Channell et al., Chap. 10, this volume). This interpretation is apparently in conflict with the biostratigraphic interpretation by Eidvin and Nagy (Chap. 1, this volume), who suggest that their uppermost analyzed level at 647 mbsf is older than 2.4 Ma. They base their dating on correlation with well-dated planktonic foraminiferal zones in boreholes from Legs 104 and 151 (Eldholm, Thiede, Taylor, et al., 1989; Thiede, Myhre, Firth, et al., 1996), as well as in the southwest Barents Sea (Eidvin et al., 1993; Eidvin et al., 1998).

The present data are not adequate to resolve this discrepancy. Reworking of the analyzed calcareous fossils could give one explanation, but according to Eidvin and Nagy (Chap. 1, this volume), few of the planktonic foraminifers show signs of wear. Less than 200 k.y. is, however, a very short time for deposition of the >300 m of sediment below Eidvin and Nagy's (Chap. 1, this volume) uppermost analyzed interval (at 647 mbsf). In the following discussion, we follow the chronology of Channell et al. (Chap. 10, this volume), which is based on the paleomagnetic results.

The base of Hole 986D, at 965 mbsf, shows reversed magnetic polarity (Shipboard Scientific Party, 1996). Occurrence of the calcareous nannofossil *P. lacunosa* further suggests an age younger than 3.6 Ma. Hence, the lower part of the cored section most likely represents the Matuyama Chron, and the base of the hole is therefore younger than 2.6 Ma. The biostratigraphic results of Eidvin and Nagy (Chap. 1, this volume) give further support to this age for the base of Hole 986D.

Ten $^{87}Sr/^{86}Sr$ analyses were performed on both planktonic and benthic foraminifers at six levels between 668 and 892 mbsf (Table 3; Fig. 8). Despite the scatter, the Sr vs. age data strongly indicate that the interval 900–670 mbsf is younger than ~2.6 Ma in accordance with the interpretation that the reversed polarity sequence represents the Matuyama Chron. The scatter makes it problematic to further refine the age model by Sr isotope ratios. Ongoing work to reduce analytical noise by testing specific species in selected samples may constrain this better in the future.

No firm ages can be assigned to the important seismic sequence boundaries R6 or R5, but linear interpolation would suggest ages of ~1.5 and 1.3 Ma, respectively, for these levels. Likewise, interpolating between a maximum age of 2.6 Ma at the base of the hole, and the base of the Olduvai Event at 756 mbsf, gives a tentative age of 2.3–2.4 Ma for R7. Although uncertain, this is compatible with age estimates (2.3–2.5 Ma) from seismic correlation to commercial wells in the southwestern Barents Sea (Faleide et al., 1996). Because of the debris flow origin of a major part of the sediments, however, any interpolation is very uncertain. Most likely the deposition occurred in a stepwise manner, with rapid emplacement of debris flow deposits and longer periods dominated by hemipelagic deposition. Such a pattern is also indicated by the grain-size distribution record (Fig. 2), as well as the zonation of reworked and in situ agglutinated benthic foraminifers (Eidvin and Nagy, Chap. 1, this volume). However, given both the spatial and temporal variability in debris flow deposition as well as the sparse age control, linear interpolation over relatively long time spans is currently our only means of estimating ages for the main seismic sequence boundaries.

Temperature Gradient and Mineralogy

The mineralogy does not seem to have undergone any diagenetic changes, which is surprising when considering the depth of burial and a geothermal gradient of 150°C/km measured by the Shipboard Scientific Party (1996). The temperature measurements were taken in the upper 60 m of the sediments, and there may be errors when projecting this gradient downward. An indication that the extrapolated temperatures may be in error comes from Rock-Eval pyrolysis analysis from 955.67 mbsf, where kerogen with a T_{max} of 427°C and an S1/(S1+S2) ratio of 0.071 was present (Shipboard Scientific Party, 1996). Both of these values indicate immature kerogen and sediment temperatures below the oil generation window (60°–100°C; Tissot and Welte, 1984). However, kinetic effects may influence kerogen maturation (Tissot and Welte, 1984). The quality of the temperature measurements appears to be good, however, and a good linear fit of temperature vs. depth was obtained (Shipboard Scientific Party, 1996). The decreasing salinity (down to 23 g/L at 883.95 mbsf) with a low content of potassium (1.3–1.9 mM below 528.15 mbsf; Shipboard Scientific Party, 1996) may have stabilized smectite with respect to illite, a transformation that is expected to occur under normal conditions at temperatures between 60° and 100°C (Hower et al., 1976; Pearson and Small, 1988). The occurrence of brackish pore water (Shipboard Scientific Party, 1996) is a problem that will be addressed in more detail in a future work. One speculation is that the sediments deposited by the meltwater rivers from glaciers in the Barents Sea region may have contained brackish pore water. If these sediments are the source of the debris flows associated with Unit III and Subunit IVA, they may have flowed as plug flows and retained their original brackish pore water, thus bringing it downslope. Other alternatives include artesian water circulation resulting from groundwater heads under temperate glaciers and diagenetic reactions other than

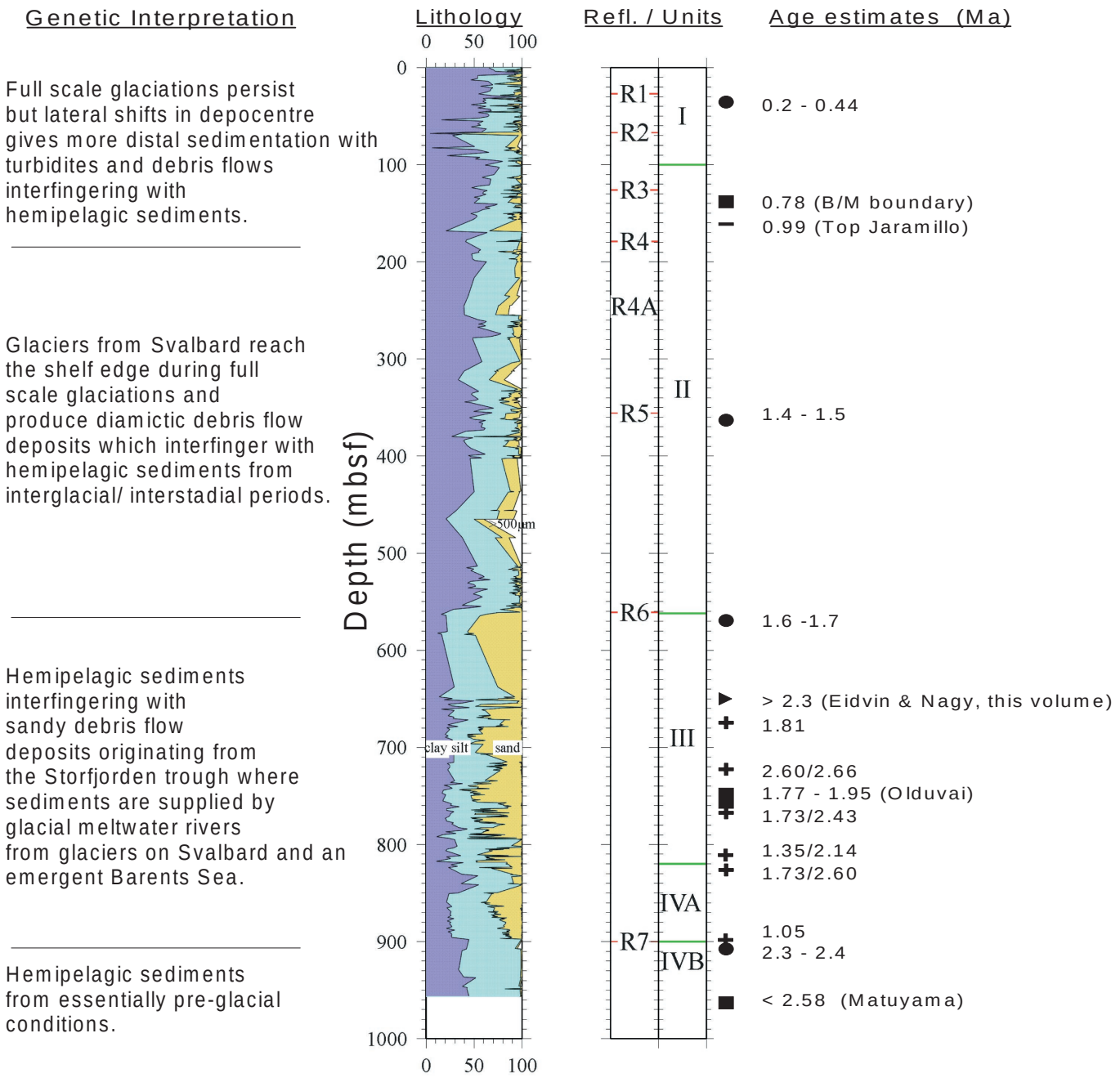

Figure 8. The present status of age determinations for Site 986. Solid rectangles indicate paleomagnetic datums, solid circles mark interpolated ages, the solid triangle represents the uppermost sample studied in the foraminiferal work by Eidvin and Nagy (Chap. 1, this volume), and crosses mark ages inferred from Sr isotopic analyses, using the data from Howarth and McArthur (1997) for conversion to ages. Single numbers mark analyses of planktonic foraminifers, whereas a slash divides dates of planktonic (first) from those of benthic (last) foraminifers. Because no continuous paleomagnetic record was obtainable, the interpretations of the top Jaramillo and Olduvai Events are debatable. Note also the apparent conflict with the biostratigraphic results of Eidvin and Nagy (Chap. 1, this volume). The age interval for R1 is based on extrapolation from a piston core (Elverhøi et al., 1995b) (youngest age) and correlation with a shallow, geotechnical borehole in the southwestern Barents Sea (Sættem et al., 1992).

the smectite-to-illite transition in the sediments. We are under the impression, however, that no major mineralogical changes have occurred since deposition. Whether this is caused by kinetic effects (i.e., 2.3 m.y. is too short a time), fresh pore water, both of these, or a third mechanism is yet to be investigated.

CONCLUSIONS

The following conclusions are also summarized in Figure 8. Site 986 documents the geological development of the west Spitsbergen margin from the late Pliocene to the present.

Early (2.6–2.4 Ma) sedimentation was dominated by hemipelagic mud deposition. The initial (2.4–2.3 Ma) glacial buildup on land is recorded through a great increase in the input of sand, but not clasts, within the sediments at Site 986. The sand is attributed to glacial erosion of Svalbard and a partially emergent Barents Sea. Sediments were fluvially transported to the coast, and downslope transport was as debris flows and/or turbidites. Debris flow deposits from this period are separated by hemipelagic sediments.

The buildup of glaciers on the continental shelf is evidenced by the persistent appearance of clasts in the sedimentary column above 560 mbsf (i.e., since ~1.6–1.7 Ma). Massive diamictic, carbonate-rich, and smectite-poor debris flows were produced by these first large glacial advances. Although no abrupt sedimentological changes are seen at ~350 mbsf (Reflector R5, 1.4–1.5 Ma), there is a change in the hemipelagic component in the sediments at about this depth. The clay mineral composition of the clay-sized fraction is dominated by smectite below this depth, whereas a mixture of smectite-rich and smectite-poor sources is evident after this level. This is interpreted as indicating the increasing importance of Svalbard as a source area (also during the hemipelagic intervals).

Debris flow deposition at Site 986 continued up to 220 mbsf (~1.2 Ma). Above this level the clast content is reduced, and the clay content increased. The change in sedimentary facies indicates a more distal setting as the depocenters migrated. Hemipelagic sediments were deposited between the flows.

ACKNOWLEDGMENTS

This research has been funded by the Norwegian Research Council (NFR) under grant numbers 110587/410 and 116425/410, Norwegian Polar Institute contribution number 325. Figures 1A, 2, 3 4, 5, and 6 were produced using the Generic Mapping Tools (Wessel and Smith, 1995).

REFERENCES

Aksu, A.E., and Hiscott, R.N., 1992. Shingled Quaternary debris flow lenses on the north-east Newfoundland slope. *Sedimentology,* 39:193–206.

Andersen, E.S., Solheim, A., and Elverhøi, A., 1994. Development of a glaciated Arctic continental margin exemplified by the western margin of Svalbard. *In* Thurston, D.K., and Fujita, K. (Eds.), *Proc. Int. Conf. on Arctic Margins.* U.S. Dept. of the Interior, Mineral Management Service, Alaska Outer Shelf Region, OCS Study, MMS 94-0040, 155–160.

Bouma, A.H., and Hollister, C.D., 1973. Deep ocean basin sedimentation. *In Turbidites and Deep Water Sedimentation.* Soc. Econ. Paleontol. Mineral., Pacific Sect., Short Course, 79–118.

Bråten, B.I., 1997. Cenozoic uplift and erosion in the western Barents Sea [Master's thesis]. Univ. Oslo. (In Norwegian.)

Cande, S.C., and Kent, D.V., 1995. Revised calibration of the geomagnetic polarity timescale for the Late Cretaceous and Cenozoic. *J. Geophys. Res.,* 100:6093–6095.

Eidvin, T., Goll, R.M., Grogan, P., Smelror, M., and Ulleberg, K., 1998. The Pleistocene to middle Eocene stratigraphy and geological evolution of the western Barents Sea continental margin at well site 7316/5-1 (Bjørnøya West area). *Nor. Geol. Tidsskr.,* 78:99–123.

Eidvin, T., Jansen, E., and Riis, F., 1993. Chronology of Tertiary fan deposits off the western Barents Sea: implications for the uplift and erosion history of the Barents shelf. *Mar. Geol.,* 112:109–131.

Eidvin, T., and Riis, F., 1989. Nye dateringer av de tre vestligste borehullene i Barentshavet. Resultater og konsekvenser for den tertiære hevningen. *Nor. Petrol. Direct.,* 27.

Eiken, O., and Hinz, K., 1993. Contourites in the Fram Strait. *Sediment. Geol.,* 82:15–32.

Eldholm, O., Thiede, J., Taylor, E., et al., 1987. *Proc. ODP, Init. Repts.,* 104: College Station, TX (Ocean Drilling Program).

Elverhøi, A., Andersen, E.S., Dokken, T., Hebbeln, D., Spielhagen, R., Svendsen, J.I., Sørflaten, M., Rørnes, A., Hald, M., and Forsberg, C.F., 1995a. The growth and decay of the Late Weichselian ice sheet in western Svalbard and adjacent areas based on provenance studies of marine sediments. *Quat. Res.,* 44:303–316.

Elverhøi, A., Svendsen, J.I., Solheim, A., Andersen, E.S., Milliman, J.M., Mangerud, J., Hald, M., and Hooke, R.LeB., 1995b. Late Quaternary sediment yield from the high arctic Svalbard area. *J. Geol.,* 103:1–17.

Faleide, J.I., Solheim, A., Fiedler, A., Hjelstuen, B.O., Andersen, E.S., and Vanneste, K., 1996. Late Cenozoic evolution of the western Barents Sea-Svalbard continental margin. *Global Planet. Change,* 12:53–74.

Farrell, J.W., Clemens, S.C., and Gromet, L.P., 1995. Improved chronostratigraphic reference curve of late Neogene seawater $^{87}Sr/^{86}Sr$. *Geology,* 23:403–406.

Fiedler, A. and Faleide, J.I., 1996. Cenozoic sedimentation along the southwestern Barents Sea margin in relation to uplift and erosion of the shelf. *Global Planet. Change,* 12:75–3.

Flood, B., Nagy, J., and Winsnes, T.S., 1971. Geological map of Svalbard 1:500 000. Sheet 1G, Spitsbergen southern part. *Norsk Polarinst. Skrif.,* 154A.

Forsberg, C.F., 1983. Sedimentation and early diagenesis of the late Quaternary deposits in the central Barents Sea [Thesis]. Univ. Oslo.

Hiscott, R.N., and Aksu, A.E., 1994. Submarine debris flows and continental slope evolution in front of Quaternary ice sheets, Baffin Bay, Canadian Arctic. *AAPG Bull.,* 78:445–460.

Hjelstuen, B.O., Elverhøi, A., Faleide, J.I., 1996. Cenozoic erosion and sediment yield in the drainage area of the Storfjorden Fan. In Solheim, A., Riis, F., Elverhoi, A., Faleide, J.I., Jensen, L.N., and Cloetingh, S. (Eds.), Impact of Glaciations on Basin Evolution: Data and Models from the Norwegian Margin and Adjacent Areas. *Global Planet. Change,* 12:95–117.

Hodell, D.A., Mueller, P.A., and Garrido, J.R., 1991. Variations in the strontium isotopic composition of seawater during the Neogene. *Geology,* 19:24–27.

Hooke, R.LeB., and Elverhøi, A., 1996. Sediment flux from a fjord during glacial periods, Isfjorden, Spitsbergen. *Global Planet. Change,* 12:237–249.

Howarth, R.J., and McArthur, J.M., 1997. Statistics for strontium isotope stratigraphy: a robust LOWESS fit to the marine Sr-isotope curve for 0 to 260 Ma, with look-up table for the derivation of numerical age. *J. Geol.,* 105:441–456.

Howe, J.A., Stoker, M.S., and Stow, D.A.V., 1994. Late Cenozoic sediment drift complex, northeast Rockall Trough, North Atlantic. *Paleoceanography,* 9:989–999.

Hower, J., Eslinger, E.V., Hower, M.E., and Perry, E.A., 1976. Mechanism of burial metamorphism of argillaceous sediment. 1. Mineralogical and chemical evidence. *Geol. Soc. Am. Bull.,* 87:725–737.

Jansen, E., and Sjøholm, J., 1991. Reconstruction of glaciation over the past 6 Myr from ice-borne deposits in the Norwegian Sea. *Nature,* 349:600–603.

King, E.L., Sejrup, H.P., Haflidason, H., Elverhøi, A., and Aarseth, I., 1996. Quaternary seismic stratigraphy of the North Sea Fan: glacially fed gravity flow aprons, hemipelagic sediments, and large submarine slides. *Mar. Geol.,* 130:293–315.

Laberg, J.S, and Vorren, T.O., 1995. Late Weichselian submarine debris flow deposits on the Bear Island trough mouth fan. *Mar. Geol.,* 127:45–72.

Mørk, M.B.E., and Duncan, R.A., 1993. Late Pliocene basaltic volcanism on the Western Barents Shelf margin: implications from petrology and ^{40}Ar-^{39}Ar dating of volcaniclastic debris from a shallow drill core. *Nor. Geol. Tidsskr.,* 73:209–225.

Pearson, M.J., and Small, J.S., 1988. Illite-smectite diagenesis and paleotemperatures in northern North Sea Quaternary to Mesozoic shale sequences. *Clay Miner.,* 23:109–132.

Pfirman, S.L., Colony, R., Nuernberg, D., Eicken, H., and Rigor, I., 1997. Reconstructing the origin and trajectory of drifting Arctic Sea ice. *J. Geophys. Res.*, 10212575–12586.

Rasmussen, E., and Fjeldskaar, W., 1996. Quantification of the Pliocene–Pleistocene erosion of the Barents Sea from present-day bathymetry. *Global Planet. Change*, 12:119–133.

Reading, H.G., and Richards, M., 1994. Turbidite systems in deep-water basin margins classified by grain size and feeder system. *AAPG Bull.*, 78:792–822.

Sættem, J., Bugge, T., Fanavoll, S., Goll, R.M., Mørk, A., Mørk, M.B.E., Smelror, M., and Verdenius, J.G., 1994. Cenozoic margin development and erosion of the Barents Sea: core evidence from southwest of Bjørnøya. *Mar. Geol.*, 118:257–281.

Sættem, J., Poole, D.A.R., Ellingsen, L., and Sejrup, H.P., 1992. Glacial geology of outer Bjornoyrenna, southwestern Barents Sea. *Mar. Geol.*, 103:15–51.

Sejrup, H.P., King, E.L., Aarseth, I., Haflidason, H., and Elverhøi, A., 1996. Quaternary erosion and depositional processes: western Norwegian fjords, Norwegian Channel and North Sea Fan. *J. Geol. Soc. London*, 117:187–202.

Shipboard Scientific Party, 1996. Site 986. In Jansen, E., Raymo, M.E., Blum, P., et al., *Proc. ODP, Init. Repts.*, 162: College Station, TX (Ocean Drilling Program), 287–343.

Solheim, A., Andersen, E.S., Elverhoi, A., and Fiedler, A., 1996. Late Cenozoic depositional history of the western Svalbard continental shelf, controlled by subsidence and climate. *Global Planet. Change*, 12:135–148.

Solheim, A., Faleide, J.I., Andersen, E.S., Elverhøi, A., Forsberg, C.F., Vanneste, K., Uenzelmann-Neben, G., and Channell, J.E.T., 1998. Late Cenozoic seismic stratigraphy and geological development of high latitude glacial continental margins: East Greenland and Svalbard–Barents Sea. *Quat. Sci. Rev.*, 17:155–184.

Thiede, J., Myhre, A.M., Firth, J.V., Johnson, G.L., and Ruddiman, W.F. (Eds.), 1996. *Proc. ODP, Sci. Res.*, 151: College Station, TX (Ocean Drilling Program).

Tissot, B.P., and Welte, D.H., 1984. *Petroleum Formation and Occurrence* (2nd ed.): Heidelberg (Springer-Verlag).

Vorren, T.O., and Laberg, J.S., 1997. Trough mouth fans: palaeoclimatic and ice-sheet monitors. *Quat. Sci. Rev.*, 16:865–881.

Wessel, P., and Smith, W.H.F., 1995. New version of the Generic Mapping Tools released. *Eos*, 76:329.

Date of initial receipt: 4 September 1997
Date of acceptance: 23 July 1998
Ms 162SR-032